nature nanotechnology

ARTICLES

PUBLISHED ONLINE: 26 FEBRUARY 2012 | DOI: 10.1038/NNANO.2012.7

A protein transistor made of an antibody molecule and two gold nanoparticles

Yu-Shiun Chen[1], Meng-Yen Hong[2] and G. Steven Huang[2]*

A major challenge in molecular electronics is to attach electrodes to single molecules in a reproducible manner to make molecular junctions that can be operated as transistors. Several attempts have been made to attach electrodes to proteins, but these devices have been unstable. Here, we show that self-assembly can be used to fabricate, in a highly reproducible manner, molecular junctions in which an antibody molecule (immunoglobulin G) binds to two gold nanoparticles, which in turn are connected to source and drain electrodes. We also demonstrate effective gating of the devices with an applied voltage, and show that the charge transport characteristics of these protein transistors are caused by conformational changes in the antibody. Moreover, by attaching CdSe quantum dots to the antibody, we show that the protein transistor can also be gated by an applied optical field. This approach offers a versatile platform for investigations of single-molecule-based biological functions and might also lead to the large-scale manufacture of integrated bioelectronic circuits.

The electronic properties of an isolated protein molecule depend on its orientation[1–3], and because most proteins maintain their native structures only in physiological media, measurements are only meaningful when the protein has a well-defined orientation and is in a hydrated form[4,5]. Scanning tunnelling microscopes (STMs)[4,6,7] and atomic force microscopes (AFMs)[5,8–12] have been used to measure the electrical conductance of self-assembled monolayers or single molecules of proteins. For example, the STM break-junction approach[13] has been used to probe electron transport in a variety of organic molecules[3,14–17]. An STM can also be used to measure the electrical properties of molecules attached to a metal substrate[18–21], and this method has been used to study proteins such as azurin[4,6,12,22], bacteriorhodopsin[2,22], yeast cytochrome *c* (ref. 9) and ferritins[8,11].

Based on analyses of electronic coupling strengths, it has been suggested that the efficiency of long-range electron transfer in proteins depends on their secondary structure. In particular, structures called sheets appear to mediate coupling more efficiently than helical structures (even though hydrogen bonds have a critical role in both structures[18]). These studies suggest that it might be possible to modulate the charge transfer properties of proteins—and thus make a protein field-effect transistor—by manipulating their secondary structure.

Attempts have been made to integrate protein monolayers into electronic devices[23–27]. For example, photosynthetic protein complexes have been integrated into organic self-assembled monolayers on gold surfaces in solid-state electronic devices[24], and the orientation of the proteins is controlled by specific binding of polyhistidine-tag-Ni^{2+} to the monolayers. Internal quantum efficiencies of ~12% have been achieved for photodetectors and photovoltaic cells. A protein thin-film transistor consisting of a 100 nm nanogap coated with an azurin monolayer[25] has also been constructed, but the current–voltage (*I*–*V*) performance deteriorates over time, probably due to an unstable molecular junction between the electrode and protein. A vertical-type molecular transistor made with a 4 nm channel and a bovine serum albumin monolayer between the source and drain electrodes has shown high gate sensitivity[27].

Attempts to construct a single-molecule protein device have led to the fabrication of a large-scale nanojunction array that serves as a framework for azurin molecule adaptation[26]. The nanojunction, which has a nanogap of ~5 nm and azurin immobilized on the bottom electrode via a disulphide bridge, is claimed to be able to integrate a single protein molecule between the electrodes.

It is now technically possible to achieve electrical contact between both sides of a protein, but, in the absence of specific binding, forcing an electrode or AFM tip into a protein can cause unpredictable denaturation of the protein that, in many instances, results in inconsistent electron transfer. Furthermore, to achieve large-scale fabrication of molecular devices, the ability to reliably self-assemble the molecular junction is an important consideration.

In this work we use self-assembly between an antibody and antigen to make molecular junctions. We have previously isolated an immunoglobulin G (IgG) antibody that recognizes 5-nm-diameter gold nanoparticles[28,29]. We allowed this anti-nanoparticle IgG to bind to two gold nanoparticles to form a junction. IgG is a Y-shaped molecule that contains three separate domains: two Fab fragments (the 'arms' of the molecule) and an Fc fragment (the stalk of the Y shape). The Fab is connected to each Fc by a flexible hinge of 12–19 amino acids, which allows the IgG molecules to bind to a broad range of antigens. This means that it is possible to form a stable protein-to-metal junction between the IgG and the electrodes, which could be particularly useful in the creation of protein transistors.

Fabrication and characterization of a protein transistor

Electron microscopy provided structural information on the gold nanoparticle–immunoglobulin complex (NP–IgG). Because the protein components could not be observed easily, we incorporated CdSe quantum dot-conjugated goat anti-mouse IgG (QD–IgG′) to assist in visualizing the NP–IgG complex. Binding complexes of NP–IgG and QD–IgG′ were examined using electron microscopy (Fig. 1a). The nanoparticles and quantum dots appear as solid spheres with diameters of 5 nm and 3 nm, respectively, and the protein components appear as a blurred mass. IgG can bind two nanoparticles, forming a NP–IgG–NP dimer. Each complex consists

[1]Biomedical Electronics Translational Research Center, National Chiao Tung University, 1001 University Road, Hsinchu, Taiwan, ROC,
[2]Department of Materials Science and Engineering, National Chiao Tung University, 1001 University Road, Hsinchu, Taiwan, ROC.
*e-mail: gstevehuang@mail.nctu.edu.tw

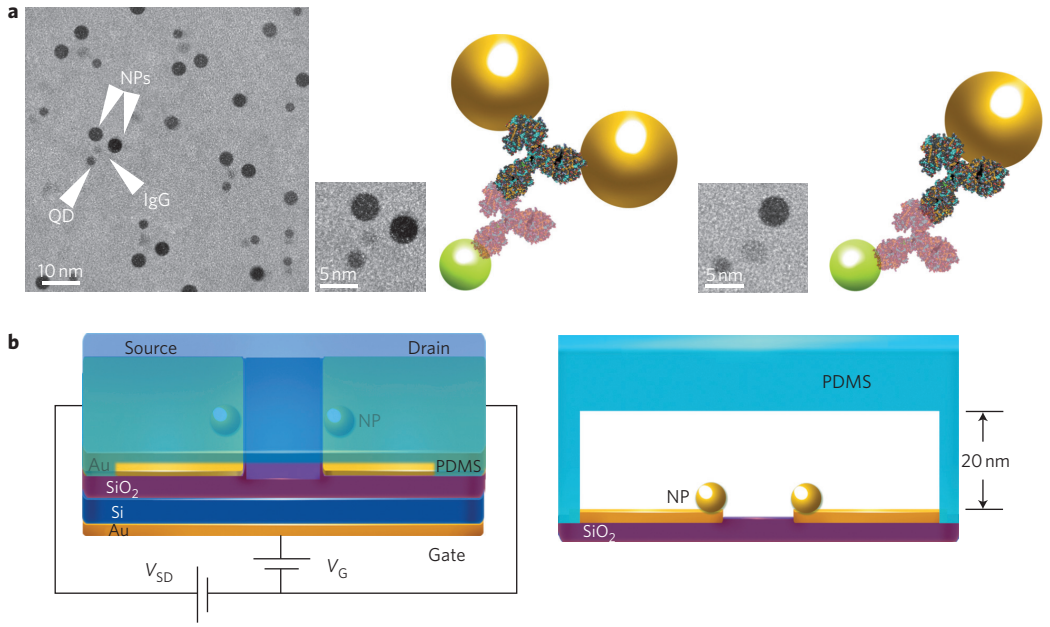

Figure 1 | Fabrication of the protein transistor. a, Left: TEM image showing the quantum dot-conjugated IgG antibody (seen as a blurred shadow) bound to two gold nanoparticles (NPs; diameter, 5 nm). Middle and right: TEM images and schematics showing the quantum dot (green)-conjugated secondary antibody (pink) bound to the F_c domain of the IgG (blue), which in turn could bind via its Fab domains to either two nanoparticles to form the NP–IgG–NP dimer (middle) or to one nanoparticle to form a monomer (right). Quantum dot diameter, 3 nm. **b**, Left: schematic representation of the protein transistor. The device is covered by PDMS to form a liquid channel (100 nm wide and 20 nm deep) and for protection. Right: front view of the liquid channel illustrating the relative positions of the gold nanoparticles and electrodes.

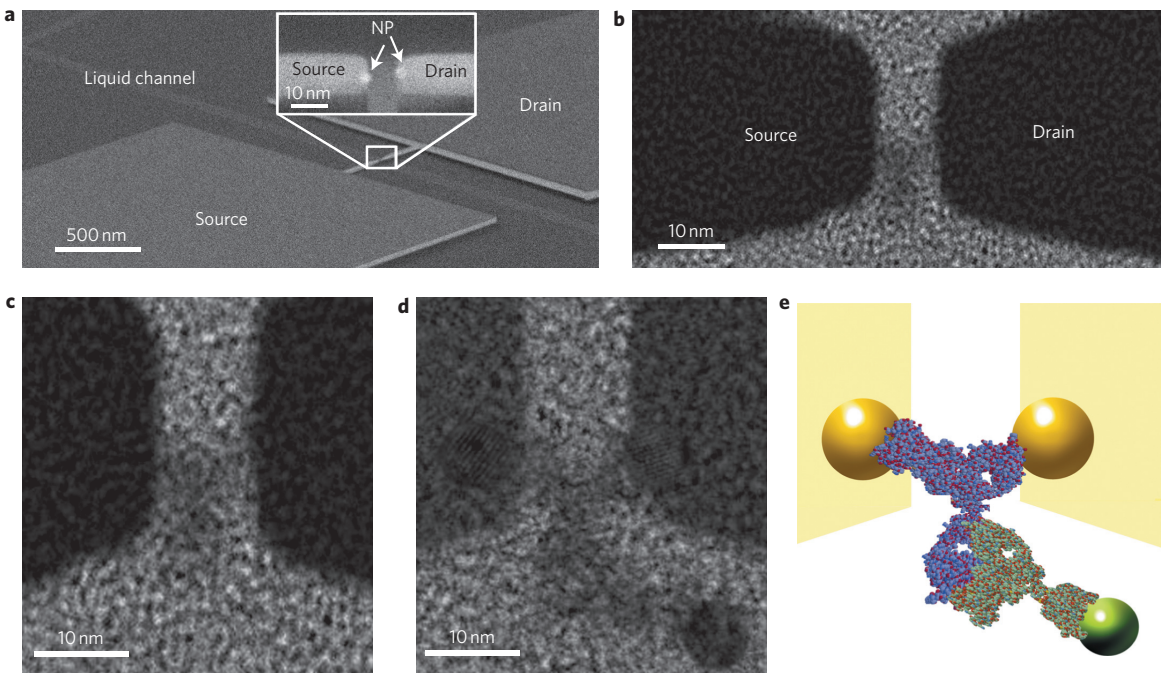

Figure 2 | Electron micrographs of the protein transistor. a, SEM image of the protein transistor. Source and drain are separated by ~10 nm. IgG binds to gold nanoparticles on top of the electrodes. Inset: two nanoparticles positioned on the electrodes. **b**,**c**, TEM images showing detailed structure of the protein transistor. IgG (seen as a blurred shadow) sits between the source and drain electrodes. **d**, TEM image showing the incorporation of quantum dot-conjugated IgG antibody (QD–IgG′) into the protein transistor. The thickness of the electrodes is processed to 5 nm to visualize the nanoparticles sitting on the electrodes. **e**, Schematic showing one possible molecular arrangement of the IgG–QD–IgG′ complex of **d**.

of three basic components: a grey protein mass of immunoglobulins at the centre, two gold nanoparticles as the two arms, and a quantum dot as the stalk. IgG is bound to the gold nanoparticle via the Fab region of the IgG molecule, and one Fab is bound with one gold nanoparticle. The distance between the two nanoparticles is ~10 nm (ref. 29).

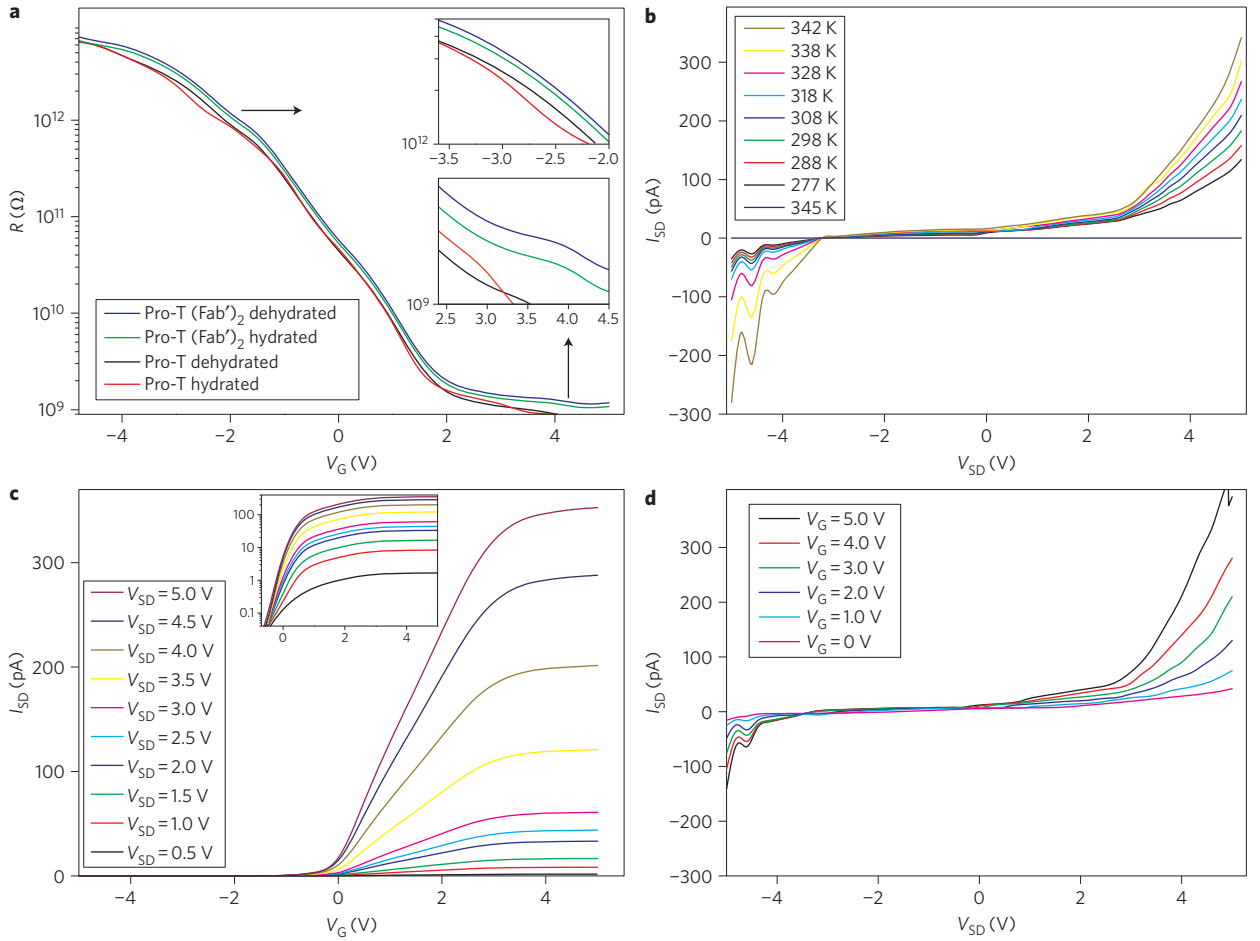

Figure 3 | Transfer characteristics of the protein transistor. a, Resistance versus voltage plot for the protein transistor in hydrated (red) and dehydrated (black) forms. When the Fc domain of pro-T is enzymatically removed (pro-T $(Fab')_2$), resistance versus voltage is also measured for hydrated (green) and dehydrated (purple) forms. **b**, I_{SD} versus V_{SD} for the protein transistor at different temperatures, showing that the current increases at higher temperatures. V_G is set at 3.0 V. **c**, I_{SD} versus V_G for different V_{SD}. The inset shows the same I_{SD} versus V_G plot with I_{SD} in logarithmic scale. **d**, I_{SD} versus V_{SD} plot for different V_G at 298 K.

Alternatively, IgG might bind a single nanoparticle, forming a NP–IgG monomer (Fig. 1a). IgG in a dimeric form would bridge two electrodes, forming a functional protein transistor, so this type of binding is preferred. Immunoprecipitation of the nanoparticles and IgG performed at various temperatures indicated that the ratio of dimer/monomer complexes formed was temperature-dependent (Supplementary Fig. S1). Binding reactions carried out at low temperatures favoured the formation of dimers; 80% dimers were formed at 15 °C and 65% at 25 °C (Supplementary Fig. S2).

A framework for the fabrication of a protein transistor was proposed (Fig. 1b). This scheme includes the fabrication of nanogaps, deposition of gold nanoparticles on the electrodes, and binding of IgG molecules to the electrodes. Electron-beam lithography was used to define nanogaps with 50-nm-wide electrodes separated by 10 nm. Nanoparticles (diameter, 5 nm) were brought onto the edge of the selected electrode pairs with the AFM tip. The nanoparticle-charged device was covered by polydimethylsiloxane (PDMS) with a pre-moulded liquid channel to protect the device from physical damage. The immunoglobulin was delivered by passing 1 pg ml^{-1} of anti-nanoparticle IgG through the liquid channel at a flow rate of 0.1 μl s^{-1}. The assembly of a protein transistor was accomplished when a stable source–drain current (I_{SD}) was detected ($I_{SD} \approx 50$ pA). An assembly rate of ~71% was achieved (Supplementary Fig. S3).

To verify the proper assembly of the single-molecule protein transistor, the IgG-loaded device was processed to its lamellar form and examined under a transmission electron microscope (TEM). The TEM image showed the presence of a single protein bridging two electrodes (Fig. 2a–c). The device was also labelled with QD–IgG′ (Fig. 2d). The TEM image clearly shows that the gold nanoparticles were present on top of each electrode. Between the two nanoparticles, a blurred mass can be seen bridging the pair. As expected, QD–IgG′ bound to the blurred mass. The composition of the quantum dot was verified by energy-dispersive X-ray spectroscopy to be cadmium and selenium (Supplementary Fig. S4). Figure 2e shows a possible arrangement of the nanoparticles, IgG and QD–IgG′ that is consistent with these observations.

We measured the resistance of IgG in the presence and absence of water (Fig. 3a). To measure the resistance in the absence of water, a vacuum of 1×10^{-7} torr was applied, but no significant difference was found in the resistance profile. The resistance of the dehydrated protein transistor was measured after 2 weeks of storage at 15 °C and remained unchanged.

Hydration of the protein might contribute to the conductivity of the protein transistor. According to this idea, an electron may have been transferred across the surface of the IgG in the adsorbed water layer. However, the conductivities of IgG in the presence and absence of water were identical, so the observed current was not caused by surface conductance. Because IgG is composed of three isolated domains, two Fabs and one Fc, the current could pass from the source electrode via one Fab, short-circuit through

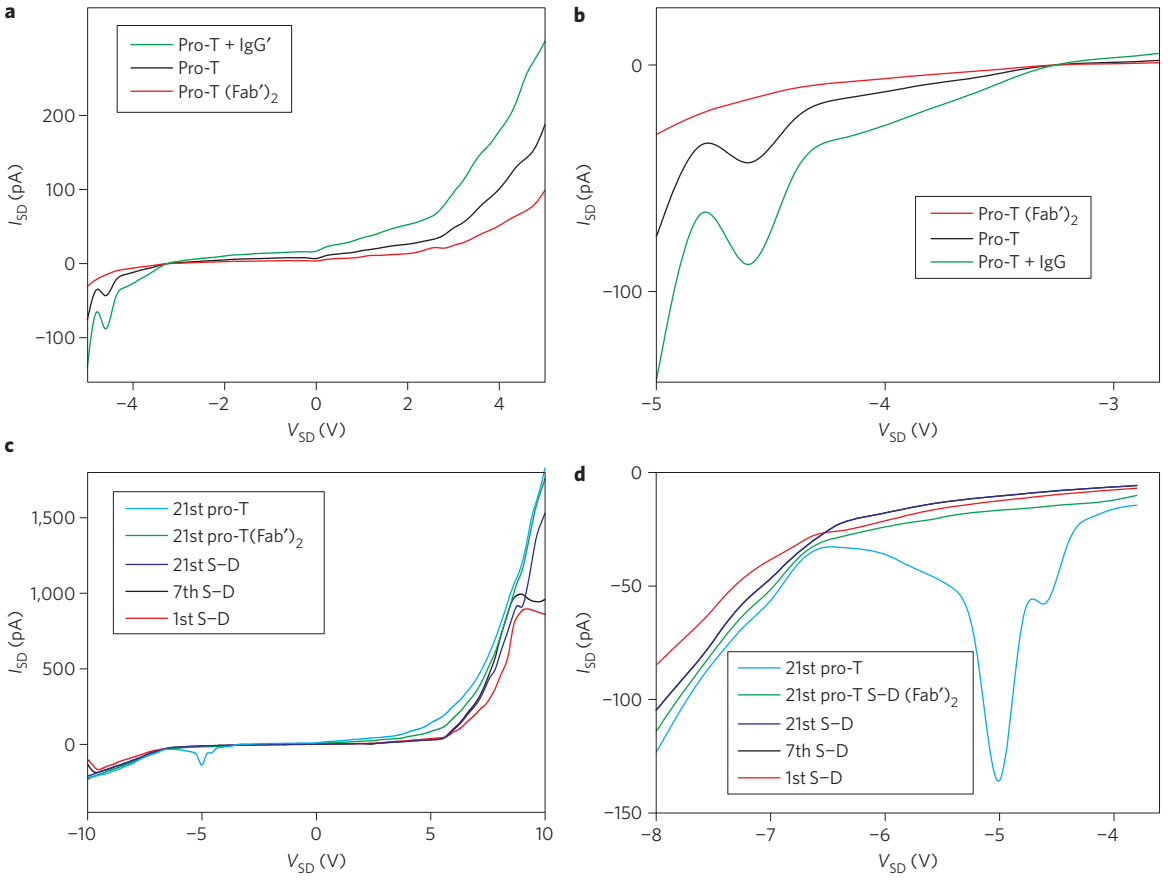

Figure 4 | Effect of the Fc domain on the NDR of pro-T. a, I_{SD} versus V_{SD} characteristics of the protein transistor in the absence of the Fc domain (pro-T $(Fab')_2$, red), for intact pro-T (pro-T, black) and pro-T bound to a secondary antibody (pro-T + IgG′, green). **b**, I_{SD} versus V_{SD} characteristics expanded from **a** for V_{SD} from −5 to −3 V. **c**, Transfer characteristics of pro-T in the absence of SiO_2 soft breakdown. The soft breakdown is removed by scanning the empty device 21 times with V_{SD} ranging from −10 V to +10 V. I_{SD} versus V_{SD} for the empty device for the first scan (1st S-D, red), seventh scan (7th S-D, black), and 21st scan (21st S-D, purple) and I_{SD} characteristics performed for the IgG-loaded device (21st pro-T, blue) and pro-T without the Fc domain (21st pro-T $(Fab')_2$, green). **d**, I_{SD} versus V_{SD} characteristics expanded from **c** for V_{SD} from −4 to −8 V.

hinges that contact the other Fab domain, and pass back to the drain electrode. This specific current passage seems unlikely because pepsin digestion, which cleaves the Fc fragment and leaves two Fab fragments connected to each other, reduced the conductivity of intact IgG by ∼50%.

The transport characteristics of the protein transistor were then measured. Figure 3b shows the dependence of I_{SD} on source–drain voltage (V_{SD}) when the gate–drain voltage (V_{GD}) was set at 3 V, for measurements performed between 277 and 345 K. In this plot, the current is seen to increase as the temperature rises. However, the device ceased to function at 345 K, probably due to thermal damage to the Fab at the nanoparticle junction, resulting in a loss of connection.

For positive bias, a threshold voltage of 2.6 ± 0.86 V was observed. Negative differential resistance (NDR) occurred at $V_{SD} = -4.2 \pm 0.22$ and -4.6 ± 0.18 V. NDR can occur when carriers are transferred from a high-mobility valley to a low-mobility valley or when resonant tunnelling occurs between localized states in conventional semiconductors[21,30–33]. NDR has also been demonstrated when measuring the conductance of organic compounds on a silicon wafer[34]. Electron-induced switching of oxidation–reduction states was considered a probable cause of NDR in organic compounds[30,33,35]. Immunoglobulin is not known as a redox enzyme; however, functional groups on its side chains might serve as temporary electron acceptors and cause multiple NDRs in the measurement.

The dependence of I_{SD} on V_G for V_{SD} varying from 0.5 to 5 V and at 277 K is shown in Fig. 3c. An on/off voltage at −0.5 V was observed. Figure 3d shows I_{SD} versus V_{SD} for V_G varying from 0 to 5 V.

Transconductance (g_m) is defined as the dependence of I_{SD} on gate voltage V_G at a fixed V_{SD}, and the output resistance r_o is defined as the modulation of I_{SD} by V_{SD} when V_G is kept constant. Polynomial regression was performed on the measured characteristics, yielding g_m and r_o values of 35.1 pA V^{-1} and 22.4 GΩ, respectively. The maximum voltage gain A_{Vmax} of the transistor, defined as the product of g_m and r_o, was 0.79; this is a reasonable value when compared with field-effect transistors made from polynucleotide monolayers[36] or carbon nanotubes[37,38]. The leakage current for the protein transistor at $V_G = -3$ V was 3.2 pA (Supplementary Fig. S5). This leakage current is relatively small compared to the leakage current of organic thin-film transistors[39].

Reproducibility is one of the main concerns for electronic devices that use biological materials as an integral component. Furthermore, under an applied electrical field, gold atoms could migrate[40] and generate a pinhole through IgG; this would result in poor reproducibility of the device. The I_{DS}–V_{DS} characteristics of 24 devices from different batches showed characteristic threshold voltages (2.6 ± 0.86 V) and NDRs (-4.2 ± 0.22 V; -4.6 ± 0.18 V) with small device-to-device deviation (Supplementary Figs S6, S7). The stability of the protein transistor during long-term storage was characterized using 60 devices from different batches over a period of 6 weeks (Supplementary Fig. S8). After 28 days of storage, the device yield remained at 75%.

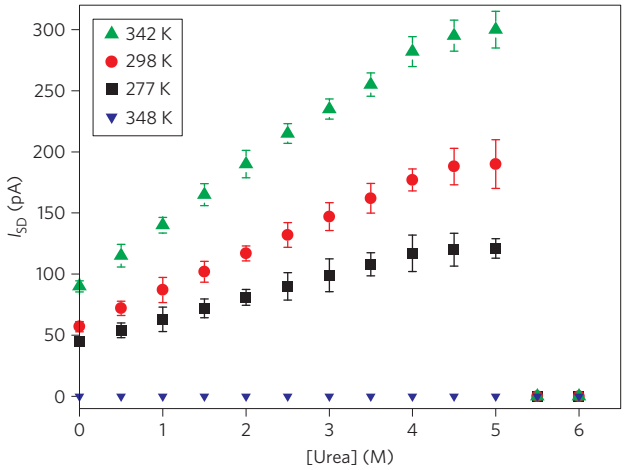

Figure 5 | Effect of urea denaturation on I_{SD} for the protein transistor. Urea denaturation of the protein transistor was performed at 277 (black squares), 298 (red circles), 342 (green triangles) and 348 K (blue triangles). Urea concentration varies from 0 to 6 M. I_{SD} is measured at $V_{SD} = 3.0$ V and $V_G = 3.0$ V. Each value is averaged from 12 independent experiments. Standard deviations are shown as error bars.

To elucidate the role of IgG, I_{SD} versus V_G was measured with the V_{SD} set at 3 V and 3.5 V (Supplementary Fig. S9). An empty protein transistor (without IgG loaded) measured with the same settings was used as a control. Step-by-step I_{SD} versus V_{SD} measurements were made after each step of fabrication for four devices (Supplementary Fig. S10). An enhanced field effect was observed after IgG loading (Supplementary Fig. S10, insets).

Characterization of the origin of NDR

To investigate the origin of the NDR, two approaches were taken: biochemical modification of IgG and SiO_2 soft breakdown. Pepsin digests the Fc domain of IgG, leaving two Fab′ domains connected by disulphide bonds; this residual fragment is referred to as $(Fab')_2$. Secondary antibodies can recognize Fc and form an IgG–IgG′ dimer. The IgG–IgG′ dimer exhibited NDR with enhanced amplitude at −4.2 and −4.6 V, without a voltage shift (Fig. 4a). However, the NDR disappeared when the Fc domain was removed by means of pepsin digestion (Fig. 4b). This result suggests that the NDR originates from the Fc domain.

The protein transistor suffered from enormous electric fields when the source and drain voltage were swept from −5 V to 5 V. In this voltage range, the SiO_2 can enter a soft break state, which was recently demonstrated to have been the cause of many previous results obtained with so-called 'molecular electronics' devices[41]. Our initial survey determined that the SiO_2 soft break state occurred at −9.0 V and +8.5 V for one of four devices (Supplementary Fig. S10). We also identified a 'third NDR' at -5 ± 0.38 V that resided at the boundary of our previous working range. For the empty device that showed soft breakdown, sweeping from −10 V to +10 V was executed repeatedly until the current fluctuation disappeared, in this case on the 21st sweep (Fig. 4c). The IgG was then loaded, and I_{SD} was measured again using $(Fab')_2$ as a control (Fig. 4d). NDRs appeared at −4.6 and −5.0 V for IgG but not for $(Fab')_2$ nor for the empty device. These results therefore show that the NDR originates from IgG, specifically from the Fc domain.

Structural and functional gating of the protein transistor

The temperature-dependent transport of the protein transistor implied that the structure of the protein within the device might play a role in its conductivity. Urea is often used as a denaturant to manipulate protein conformation in folding studies. Urea denaturation of protein transistors was carried out at 277, 298 and 342 K (Fig. 5). The observed I_{SD} was proportional to the concentration of urea and was modulated by the conformational change of IgG in the protein transistor. Saturation occurred at 4.5 and 5.0 M, beyond which further increases in urea concentration resulted in very little increase in I_{SD}. However, when the urea concentration reached 5.5 M, I_{SD} dropped to zero. If the urea concentration was reduced at this stage, the I_{SD} never recovered, indicating a permanent disruption of the device. This could be due to the complete denaturation of Fab domains and the consequent loss of electrical contact. We found that the structural gating effect was greater at 342 K (with a range of 200 pA) than at 277 K (70 pA).

The enzymatic function of the bridging protein could modulate the gating of the protein transistor. To incorporate an additional function, QD–IgG′ was attached to the F_C domain in the protein transistor. Addition of the quantum dots gave the protein transistor the ability to emit fluorescence when excited by ultraviolet light. Figure 6a shows the I–V characteristics of QD–IgG′-conjugated protein transistors. The incorporation of QD–IgG′ increased I_{SD}. Excitation using ultraviolet light sources further enhanced the I_{SD}. Horseradish peroxidase (HRP)-conjugated secondary IgG was incorporated to serve as a control for light gating (Fig. 6b). The binding of HRP–IgG′ increased the I_{SD} by 40%. Further excitation with ultraviolet light had no effect on the I_{SD} of HRP–IgG′. The performance of QD–IgG′ was gated by the wavelength of the applied ultraviolet light (Fig. 6c and Supplementary Fig. S11). The light gating ability of quantum-dot-conjugated protein transistors is

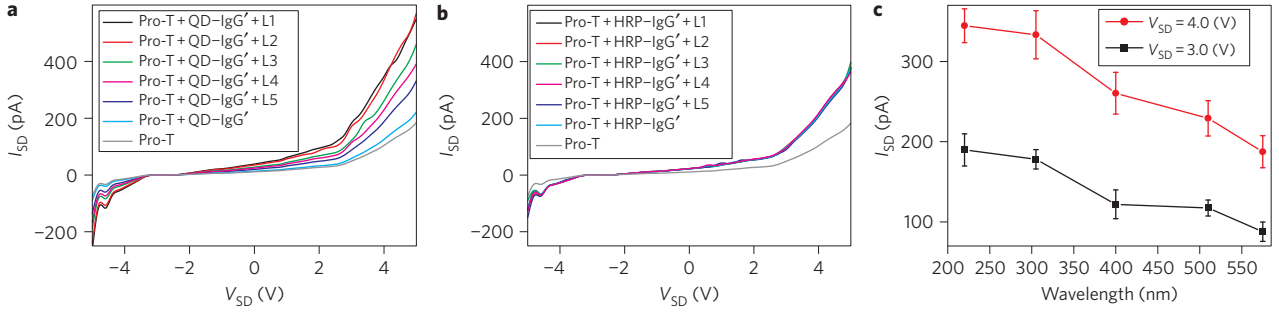

Figure 6 | Light-sensitive gating of the quantum dot-functionalized protein transistor. a, I_{SD} versus V_{SD} for QD–IgG′-conjugated pro-T irradiated by ultraviolet light with wavelengths peaked at 220 nm (L1, black), 305 nm (L2, red), 400 nm (L3, green), 510 nm (L4, pink) and 575 nm (L5, purple). Results for pro-T (grey) and QD-functionalized pro-T in the absence of ultraviolet light (blue) are also shown. **b**, I_{SD} versus V_{SD} plot of HRP–IgG′-conjugated pro-T irradiated by ultraviolet light with wavelengths peaked at 220 nm (L1, black), 305 nm (L2, red), 400 nm (L3, green), 510 nm (L4, pink) and 575 nm (L5, purple). Results for pro-T (grey) and HRP-conjugated pro-T in the absence of ultraviolet light (blue) are also shown. **c**, I_{SD} versus peaked wavelengths of ultraviolet light for V_{SD} set at 3.0 (black) and 4.0 V (red). Standard deviations are shown as error bars.

probably due to the injection of light-induced charge carriers into the conducting layer of the protein transistors. The underlying mechanism is probably photon-induced charge separation of nanocrystals followed by electron transfer to the acceptors[42].

The similarity between the observed conductivity of IgG in solution and under vacuum implied that very little physical change in the protein occurred when the protein transistor device was moved between the two conditions (Fig. 4c). This observation was surprising but not totally unexpected, because immunoglobulin has evolved as a structurally stable protein. An environment completely different from water surrounds protein when in vacuum. Based on results obtained using native mass spectrometry, proteins in the gas phase have been proposed to take on conformations that differ from their native solution structures[43]. However, recent studies using fluorescence, electron capture dissociation and electrospray ionization indicate that the structures of proteins in the gas phase are similar to those of proteins in solution[44–46]. In the gas phase, many significant features of protein structure, including hydrogen bonds and secondary structural elements, are preserved. Our observations indicate that the native structure of IgG is maintained for a significant duration when the device is moved from solution to vacuum. Because the structure of proteins in the gas phase remains a challenging research field, the present platform might provide an alternative approach to studying single-molecule protein-folding kinetics in vacuum and in solution. The timescale for the conformational change of protein ranges from microseconds to seconds[47]. In the absence of an applied voltage, electrons travel through protein on a millisecond timescale[48]. By adjusting the bias voltage and scanning frequency, it is possible to observe the fluctuation of protein conductance on a submillisecond timescale.

Methods

Nanoparticle synthesis. Gold nanoparticles (diameter, 5 nm) were synthesized as previously reported[49]. To obtain antibodies that specifically recognize nanoparticles, BALB/c mice were immunized weekly by intraperitoneal injection of adjuvant-emulsified 5 nm nanoparticles. Antiserum was obtained in the fourth week. The anti-nanoparticle binding affinity of the serum was examined by enzyme-linked immunosorbent assays[28]. IgG was further purified from antiserum containing nanoparticle-binding activity using protein A–agarose gel (Invitrogen). The affinity and specificity of the IgG for nanoparticles was further characterized by AFM (Supplementary Section II, 'AFM measurement of NP–IgG binding affinity').

Fabrication of protein transistors. Electron-beam lithography was used to define the nanogap, which consisted of 50-nm-wide electrodes separated by a gap of 10 nm. Buffered oxide etch (BOE) was used to erode the electrode area to a depth of ~100 nm. This was followed by gold deposition to fill in the electrode. A third electrode (gate) was deposited as gold/chromium on the back of the device to produce a transistor. The finished electrodes were 100–120 nm thick and ~5–10 nm above the SiO_2 plane. The electrode pairs were examined by scanning electron microscopy (SEM) to select nanogaps that were ~10 nm apart. Nanoparticles (diameter, 5 nm) were brought onto the edge of the selected electrode pairs with an AFM tip using Matlab programming to control the delivery action. The alignment key (20 nm × 20 nm square) was fabricated during electron-beam lithography. The key provides coordinates with which to search for the front ends of the source–drain electrode pairs and resides 2,000 nm from the electrode arrays. In the test run, an AFM tip carrying nanoparticles began scanning from the key and approached the gold electrodes in tapping mode (Supplementary Fig. S12). The movement of the AFM tip was perpendicular to the longitudinal axis of the electrodes (Supplementary Fig. S13a). The attractive force between the AFM tip and the silicon substrate was -361 ± 3.8 pN (Supplementary Fig. S13b, step 1). An occurrence of a higher attractive force (-788 ± 3.2 pN) indicated a change of the scanned surface from the silicon wafer to the gold electrode (Supplementary Fig. S13b, step 2), thereby allowing the location of the edges of the electrodes. In the loading run, AFM scanning was switched from tapping mode to contact mode immediately after passing the edge of the electrode when the attractive force was larger than 700 pN with a loading rate of 5 nm s^{-1}. A rapid increase in the attractive force followed by a sudden increase in the repellent force indicated successful loading of the nanoparticles onto the electrode (Supplementary Fig. S13b (step 3), S13c). Failure of nanoparticle loading was indicated by a lack of repellent force and the presence of attraction between the AFM tip and the substrate (Supplementary Fig. S13d). To avoid interference with the pre-deposited nanoparticle, we used a 20-nm-diameter AFM tip. A success rate of ~15–20% was achieved using this protocol.

The nanoparticle-charged device was covered with PDMS, which provided a liquid channel (100 nm wide and 20 nm deep) and protected the device from physical damage. Alignment of the PDMS channel and protein transistor was performed using the mask aligner (PEM-800). This was followed by setting the PDMS channel on the bottom XYZ stage and the protein transistor device on the top stage. Key positions (1 μm × 1 μm) were aligned under a light microscope followed by SEM examination to select for a device with exact alignment. IgG was then brought onto the electrodes and permitted to bind to the nanoparticles. The residual protein was washed away with PBS and then H_2O. Successful binding across two electrodes was identified by applying a bias voltage and verifying the conductivity between them.

Characteristics of the protein transistor. The current–voltage (I_{DS}–V_{DS}) characteristics were determined in a probing station in a high-vacuum test chamber with an HP4145 standard semiconductor parametric analyser (Hewlett-Packard) and a Keithley 487 power supply (Supplementary Fig. S14). The vacuum was maintained at 1×10^{-7} torr by a turbo pump. The solutions were introduced through two inlets onto the microchip using a micro-syringe pump (model 200 series; KD Scientific) at a flow rate of 6 μl min^{-1}. All measurements were performed at this flow rate. The nanoparticles adhere to the electrodes in a stable manner even with a fast flow rate of 120 μl min^{-1} for several hours of operation.

Received 27 October 2011; accepted 10 January 2012; published online 26 February 2012; corrected after print 2 March 2012

References

1. Trammell, S. A., Spano, A., Price, R. & Lebedev, N. Effect of protein orientation on electron transfer between photosynthetic reaction centers and carbon electrodes. *Biosens. Bioelectron.* **21,** 1023–1028 (2006).
2. Ron, I., Friedman, N., Cahen, D. & Sheves, M. Selective electroless deposition of metal clusters on solid-supported bacteriorhodopsin: applications to orientation labeling and electrical contacts. *Small* **4,** 2271–2278 (2008).
3. Venkataraman, L., Klare, J. E., Nuckolls, C., Hybertsen, M. S. & Steigerwald, M. L. Dependence of single-molecule junction conductance on molecular conformation. *Nature* **442,** 904–907 (2006).
4. Friis, E. P. *et al.* An approach to long-range electron transfer mechanisms in metalloproteins: *in situ* scanning tunneling microscopy with submolecular resolution. *Proc. Natl Acad. Sci. USA* **96,** 1379–1384 (1999).
5. Stamouli, A., Frenken, J. W. M., Oosterkamp, T. H., Cogdell, R. J. & Aartsma, T. J. The electron conduction of photosynthetic protein complexes embedded in a membrane. *FEBS Lett.* **560,** 109–114 (2004).
6. Alessandrini, A., Corni, S. & Facci, P. Unravelling single metalloprotein electron transfer by scanning probe techniques. *Phys. Chem. Chem. Phys.* **8,** 4383–4397 (2006).
7. Lee, I., Lee, J. W. & Greenbaum, E. Biomolecular electronics: vectorial arrays of photosynthetic reaction centers. *Phys. Rev. Lett.* **79,** 3294–3297 (1997).
8. Axford, D. N. & Davis, J. J. Electron flux through apo- and holoferritin. *Nanotechnology* **18,** 145502 (2007).
9. Delfino, I. *et al.* Yeast cytochrome *c* integrated with electronic elements: a nanoscopic and spectroscopic study down to single-molecule level. *J. Phys. Condens. Matter* **19,** 225009 (2007).
10. Reiss, B. D., Hanson, D. K. & Firestone, M. A. Evaluation of the photosynthetic reaction center protein for potential use as a bioelectronic circuit element. *Biotechnol. Progr.* **23,** 985–989 (2007).
11. Xu, D. G., Watt, G. D., Harb, J. N. & Davis, R. C. Electrical conductivity of ferritin proteins by conductive AFM. *Nano Lett.* **5,** 571–577 (2005).
12. Zhao, J. W., Davis, J. J., Sansom, M. S. P. & Hung, A. Exploring the electronic and mechanical properties of protein using conducting atomic force microscopy. *J. Am. Chem. Soc.* **126,** 5601–5609 (2004).
13. Reed, M. A., Zhou, C., Muller, C. J., Burgin, T. P. & Tour, J. M. Conductance of a molecular junction. *Science* **278,** 252–254 (1997).
14. Haick, H. & Cahen, D. Making contact: connecting molecules electrically to the macroscopic world. *Prog. Surf. Sci.* **83,** 217–261 (2008).
15. Haick, H. & Cahen, D. Contacting organic molecules by soft methods: towards molecule-based electronic devices. *Acc. Chem. Res.* **41,** 359–366 (2008).
16. Quek, S. Y. *et al.* Amine-gold linked single-molecule circuits: experiment and theory. *Nano Lett.* **7,** 3477–3482 (2007).
17. Cheng, Z. L. *et al. In situ* formation of highly conducting covalent Au–C contacts for single-molecule junctions. *Nature Nanotech.* **6,** 353–357 (2011).
18. Gray, H. B. & Winkler, J. R. Electron transfer in proteins. *Annu. Rev. Biochem.* **65,** 537–561 (1996).
19. Gray, H. B. & Winkler, J. R. Electron tunneling through proteins. *Q. Rev. Biophys.* **36,** 341–372 (2003).
20. Heath, J. R. & Ratner, M. A. Molecular electronics. *Phys. Today* **56,** 43–49 (May 2003).
21. Joachim, C. & Ratner, M. A. Molecular electronics: some views on transport junctions and beyond. *Proc. Natl Acad. Sci. USA* **102,** 8801–8808 (2005).
22. Ron, I. *et al.* Proteins as electronic materials: electron transport through solid-state protein monolayer junctions. *J. Am. Chem. Soc.* **132,** 4131–4140 (2010).

23. Carmeli, I., Frolov, L., Carmeli, C. & Richter, S. Photovoltaic activity of photosystem I-based self-assembled monolayer. *J. Am. Chem. Soc.* **129,** 12352–12353 (2007).
24. Das, R. *et al.* Integration of photosynthetic protein molecular complexes in solid-state electronic devices. *Nano Lett.* **4,** 1079–1083 (2004).
25. Maruccio, G. *et al.* Towards protein field-effect transistors: report and model of prototype. *Adv. Mater.* **17,** 816–822 (2005).
26. Maruccio, G. *et al.* Protein conduction and negative differential resistance in large-scale nanojunction arrays. *Small* **3,** 1184–1188 (2007).
27. Mentovich, E. D., Belgorodsky, B., Kalifa, I., Cohen, H. & Richter, S. Large-scale fabrication of 4-nm-channel vertical protein-based ambipolar transistors. *Nano Lett.* **9,** 1296–1300 (2009).
28. Chen, Y. S., Hung, Y. C., Chen, K. C. & Huang, G. S. Detection of gold nanoparticles using an immunoglobulin-coated piezoelectric sensor. *Nanotechnology* **19,** 495502 (2008).
29. Huang, G. S., Chen, Y. S. & Yeh, H. W. Measuring the flexibility of immunoglobulin by gold nanoparticles. *Nano Lett.* **6,** 2467–2471 (2006).
30. Chen, J., Reed, M. A., Rawlett, A. M. & Tour, J. M. Large on–off ratios and negative differential resistance in a molecular electronic device. *Science* **286,** 1550–1552 (1999).
31. Chen, J. *et al.* Room-temperature negative differential resistance in nanoscale molecular junctions. *Appl. Phys. Lett.* **77,** 1224–1226 (2000).
32. Farver, O. & Pecht, I. Long-range intramolecular electron-transfer in azurins. *J. Am. Chem. Soc.* **114,** 5764–5767 (1992).
33. Zimbovskaya, N. A. & Pederson, M. R. Negative differential resistance in molecular junctions: effect of the electronic structure of the electrodes. *Phys. Rev. B* **78,** 153105 (2008).
34. Guisinger, N. P., Greene, M. E., Basu, R., Baluch, A. S. & Hersam, M. C. Room temperature negative differential resistance through individual organic molecules on silicon surfaces. *Nano Lett.* **4,** 55–59 (2004).
35. Mentovich, E. D., Belgorodsky, B. & Richter, S. Resolving the mystery of the elusive peak: negative differential resistance in redox proteins. *J. Phys. Chem. Lett.* **2,** 1125–1128 (2011).
36. Maruccio, G. *et al.* Field effect transistor based on a modified DNA base. *Nano Lett.* **3,** 479–483 (2003).
37. Appenzeller, J. *et al.* Field-modulated carrier transport in carbon nanotube transistors. *Phys. Rev. Lett.* **89,** 126801 (2002).
38. Tans, S. J., Verschueren, A. R. M. & Dekker, C. Room-temperature transistor based on a single carbon nanotube. *Nature* **393,** 49–52 (1998).
39. DiBenedetto, S. A., Facchetti, A., Ratner, M. A. & Marks, T. J. Molecular self-assembled monolayers and multilayers for organic and unconventional inorganic thin-film transistor applications. *Adv. Mater.* **21,** 1407–1433 (2009).
40. Ramachandran, G. K. *et al.* A bond-fluctuation mechanism for stochastic switching in wired molecules. *Science* **300,** 1413–1416 (2003).
41. Yao, J., Zhong, L., Natelson, D. & Tours, J. M. Silicon oxide: a non-innocent surface for molecular electronics and nanoelectronics studies. *J. Am. Chem. Soc.* **133,** 941–948 (2011).
42. Kamat, P. V. Quantum dot solar cells. Semiconductor nanocrystals as light harvesters. *J. Phys. Chem. C* **112,** 18737–18753 (2008).
43. Wolynes, P. G. Biomolecular folding *in vacuo*!!!(?). *Proc. Natl Acad. Sci. USA* **92,** 2426–2427 (1995).
44. Breuker, K., Bruschweiler, S. & Tollinger, M. Electrostatic stabilization of a native protein structure in the gas phase. *Angew. Chem. Int. Ed.* **50,** 873–877 (2011).
45. Iavarone, A. T., Patriksson, A., van der Spoel, D. & Parks, J. H. Fluorescence probe of Trp-cage protein conformation in solution and in gas phase. *J. Am. Chem. Soc.* **129,** 6726–6735 (2007).
46. Patriksson, A., Marklund, E. & van der Spoel, D. Protein structures under electrospray conditions. *Biochemistry* **46,** 933–945 (2007).
47. Burton, R. E., Huang, G. S., Daugherty, M. A., Fullbright, P. W. & Oas, T. G. Microsecond protein folding through a compact transition state. *J. Mol. Biol.* **263,** 311–322 (1996).
48. Page, C. C., Moser, C. C. & Dutton, P. L. Mechanism for electron transfer within and between proteins. *Curr. Opin. Chem. Biol.* **7,** 551–556 (2003).
49. Brown, K. R., Walter, D. G. & Natan, M. J. Seeding of colloidal Au nanoparticle solutions. 2. Improved control of particle size and shape. *Chem. Mater.* **12,** 306–313 (2000).

Acknowledgements

This work was supported by the 'Aim for the Top University Plan' of National Chiao Tung University and the Ministry of Education, Taiwan, ROC. The authors also acknowledge funding support from the Air Force Office of Scientific Research (AFOSR, FA2386-11-1-4094).

Author contributions

Y.S.C. and G.S.H. are responsible for the study concept and design. G.S.H. and M.Y.H. prepared the manuscript. Y.S.C. and M.Y.H. carried out the experiments and performed the data analysis.

Additional information

The authors declare no competing financial interests. Supplementary information accompanies this paper at www.nature.com/naturenanotechnology. Reprints and permission information is available online at http://www.nature.com/reprints. Correspondence and requests for materials should be addressed to G.S.H.

CORRIGENDUM

A protein transistor made of an antibody molecule and two gold nanoparticles

Yu-Shiun Chen, Meng-Yen Hong and G. Steven Huang

Nature Nanotechnology **7,** 197–203 (2012); published online 26 February 2012; corrected after print 2 March 2012

In the version of this Article originally published, the address of the first affiliation was incorrect; the correct address should have read 'Biomedical Electronics Translational Research Center, National Chiao Tung University, 1001 University Road, Hsinchu, Taiwan, ROC'. This has now been corrected in the HTML and PDF versions.